HHS Public Access

Author manuscript

Exp Eye Res. Author manuscript; available in PMC 2017 April 01.

Published in final edited form as:

Exp Eye Res. 2016 April ; 145: 173–186. doi:10.1016/j.exer.2015.10.014.

Expansions of the Neurovascular Scleral Canal and Contained Optic Nerve Occur Early in the Hypertonic Saline Rat Experimental Glaucoma Model

Marta Pazos[d], **Hongli Yang**[a], **Stuart K. Gardiner**[b], **W.O. Cepurna**[c], **E.C. Johnson**[c], **J.C. Morrison**[c], and **Claude F. Burgoyne**[a]

[a]Devers Eye Institute, Optic Nerve Head Research Laboratory, Legacy Research Institute, Portland, Oregon

[b]Devers Eye Institute, Discoveries in Sight Research Laboratories, Legacy Research Institute, Portland, Oregon

[c]Kenneth C. Swan Ocular Neurobiology Laboratory, Casey Eye Institute, Oregon Health and Science University, Portland, Oregon

[d]Hospital de l'Esperança. Parc de Salut Mar. Universitat Autònoma de Barcelona, Barcelona, Spain

Abstract

Purpose—To characterize early optic nerve head (ONH) structural change in rat experimental glaucoma (EG).

Methods—Unilateral intraocular pressure (IOP) elevation was induced in Brown Norway rats by hypertonic saline injection into the episcleral veins and animals were sacrificed 4 weeks later by perfusion fixation. Optic nerve cross-sections were graded from 1 (normal) to 5 (extensive injury) by 5 masked observers. ONH's with peripapillary retina and sclera were embedded, serial sectioned, 3-D reconstructed, delineated, and quantified. Overall and animal-specific EG versus Control eye ONH parameter differences were assessed globally and regionally by linear mixed effect models with significance criteria adjusted for multiple comparisons.

Results—Expansions of the optic nerve and surrounding anterior scleral canal opening achieved statistical significance overall ($p<.0022$), and in 7 of 8 EG eyes ($p<.005$). In at least 5 EG eyes, significant expansions ($p<.005$) in Bruch's membrane opening (range 3–10%), the anterior and posterior scleral canal openings (8–21% and 5–21%, respectively), and the optic nerve at the anterior and posterior scleral canal openings (11–30% and 8–41%, respectively) were detected. Optic nerve expansion was greatest within the superior and inferior quadrants. Optic nerve expansion at the posterior scleral canal opening was significantly correlated to optic nerve damage ($R= 0.768$, $P=.042$).

Corresponding Author: Claude F. Burgoyne, MD, Devers Eye Institute, Optic Nerve Head Research Laboratory, 1225 NE 2nd Ave, Portland OR 97232. cfburgoyne@deverseye.org. Tel: +1-503-413-5441, Fax: +1-503-413-5179.
Marta Pazos and Hongli Yang are co-first authors of this work.

Conclusion—In the rat ONH, the optic nerve and surrounding Bruch's membrane opening and neurovascular scleral canal expand early in their response to chronic experimental IOP elevation. These findings provide phenotypic landmarks and imaging targets for detecting the development of experimental glaucomatous optic neuropathy in the rat eye.

Keywords

Glaucoma; Rat; Optic Nerve Head; Neural Canal; scleral canal; Optic Nerve; Proprietary Interest Category: N

Introduction

Mouse and rat experimental glaucoma models are increasingly utilized to study the mechanisms of chronic intraocular pressure-induced optic nerve injury. While the nonhuman primate experimental glaucoma model (Burgoyne, 2015b) benefits from optic nerve head (ONH) anatomy and physiology that is similar to the human ONH, the model is impractical for studies that require large sample sizes. By contrast, rodent models (Crowston et al., 2015; Fernandes et al., 2015; Morgan and Tribble, 2015; Morrison et al., 2015; Overby and Clark, 2015; Pang et al., 2015) display pathophysiologic changes that are comparable to human glaucoma, despite substantial differences in ONH anatomy.

The suitability of rodent models is based upon several lines of reasoning. First, a series of previous reports have determined that early (if not the earliest) damage to the retinal ganglion cell axons occurs within the ONH tissues in all induced and spontaneous forms of rodent (Morrison, 2005; Morrison et al., 2011; Morrison et al., 2008; Morrison et al., 1997; Morrison et al., 1998; Schlamp et al., 2006) and primate (Burgoyne et al., 2004; Downs et al., 2007; Yang et al., 2007a; Yang et al., 2007b) chronic IOP elevation. Second, to a certain degree, the rodent ONH demonstrates characteristics that are analogues to the primate ONH (Morrison et al., 2011). These include similar ultrastructural relationships between astrocytes and axons (Morrison et al., 1995; Morrison et al., 1997) as well as similar cellular changes (Hernandez et al., 1990; Johnson et al., 1996; Morrison et al., 1990), neural canal expansion (Chauhan et al., 2002; Guo et al., 2005) and posterior deformation of the ONH surface in response to chronic IOP elevation (Chauhan et al., 2002). Likewise, chronic models of IOP elevation in rats have also demonstrated a predilection for early superior optic nerve injury (Dai et al., 2012; Huang and Knighton, 2009; Li et al., 2015; Morrison, 2005; Morrison et al., 1997; WoldeMussie et al., 2001) (Morrison JC, et al. *IOVS* 2002; ARVO E-Abstract 2885). Understanding the basis for this regional susceptibility in rats may provide insight into mechanisms of regional susceptibility in humans.

Third, the anatomy of the rodent ONH is also very different from the human and non-human primate (Morrison et al., 2011). Understanding these differences and recognizing how they contribute to species-related differences in age-related retinal ganglion cell axon loss (Cepurna et al., 2005) and age-related differences in the susceptibility of axon transport to acute (Kong et al., 2009) and chronic IOP elevation (Morrison et al., 1997) (Morrison JC et al. *IOVS* 2007; 48: ARVO E-Abstract 3662; Johnson EC et al. *IOVS* 2008; 49: ARVO E-

Abstract 4059) should provide important knowledge about these same phenomena in human eyes.

We recently performed high-resolution (1.5 cubic micron voxel) 3D histomorphometric reconstruction of the optic nerve head (ONH) and peripapillary sclera from both the normal control (Control) and experimental glaucoma (EG) eyes of eight brown Norway rats that had undergone 4 weeks of unilateral chronic IOP elevation. In an initial publication (Pazos et al., 2015), we described the 3D histomorphometric anatomy of the 8 Control rat ONHs and characterized the differences between the normal control rat and primate ONH (Figures 1 – 7 of our previous report) (Pazos et al., 2015). That study was the first to describe the rat ONH as consisting of two scleral openings (a neurovascular and arterial) and clarify that the central retinal artery (CRA) does not accompany the central retinal vein (CRV) within the neurovascular canal, but passes through a separate, large, irregular opening, inferior to it, accompanied by the long posterior ciliary arteries (LCPAs) and their dense intra-scleral branches. Our study confirmed the presence of a previously described (Dai et al., 2012; Morrison et al., 1999; Sugiyama et al., 1999) vascular plexus that is continuous from the choroid to the optic nerve sheathes and surrounds the optic nerve within the neurovascular scleral canal. It additionally confirmed the anatomic proximity of the retinal ganglion cell (RGC) axon bundles and a prominent extension of Bruch's Membrane (BM) superiorly that is unique to that region.

The purpose of the present report is to 3-D characterize overall and animal specific, global and regional EG versus Control eye differences within the 8 rats of our previous report (Pazos et al., 2015).

Materials and Methods

Table 1 defines all abbreviations. Supplemental Figures 1–3 (corresponding to figures 1–3 of our previous publication (Pazos et al., 2015)) review the macroscopic and microscopic relationships of the rat ONH. See our previous report (Pazos et al., 2015) for more detailed illustration of the 3D relationships among the neural, vascular and connective components of the rat ONH. Throughout the present report, all right and left eye data are presented in right eye orientation and all *parameters* are italicized to distinguish the behavior of *measured parameters* from the behavior of the underlying anatomy they characterize (not italicized).

Animals and eyes

All animals were treated in accordance with the ARVO Statement for the Use of Animals in Ophthalmic and Vision Research. Both the Control and EG eyes of 8 adult male brown Norway rats, between 9.5 and 10.5 months of age, were studied (Table 2).

Induction of chronic unilateral experimental IOP elevation and its measurement in rats

Animals were housed initially in standard lighting conditions, with lights automatically turned on at 6 AM and off at 6 PM. One week before the hypertonic episcleral vein injection in one eye (the treated eye), each animal was placed in constant light conditions (24 hours exposure to 40–90 lux) (Morrison et al., 2005; Pang et al., 2005). Following injection, each animal was followed for 4 weeks, and then sacrificed (see below). IOP readings in both the

Control and EG eyes of each animal were made while awake (using 0.5% proparacaine hydrochloride as topical anesthesia to avoid the effects of general anesthetics) using a hand-held TonoPen tonometer. IOP was measured at least every other day, with a minimum of 14 IOP readings over the 4 weeks post saline injection. Mean IOP for both eyes of each animal was calculated as the area under the curve of an IOP vs days plot divided by the number of days. The Mean IOP Difference for each animal was defined to be the difference between the mean IOP of the EG versus the Control eye. The Peak IOP for each animal was defined to be the highest IOP in the EG eye.

Rat Euthanasia, Fixation and Injury Grade analysis

All animals were sacrificed 4 weeks post-initial saline injection to the treated eye under isoflurane anesthesia by transcardial injection of heparin (1 ml/kg) containing 10 mg ml sodium nitroprusside followed by 1 liter of 5% glutaraldehyde in 0.1 M phosphate buffer (pH 7.2). Optic nerves were dissected, washed, dehydrated and embedded in Spurr's resin as previously described (Morrison et al., 1998). Using light microscopy, 5 masked observers graded the orbital optic nerve cross-section from each eye using a previously published scale from 1 (no injury) to 5 (active degeneration involving the whole nerve area) (Jia et al., 2000) and their grades were averaged to obtain the final injury grade for each nerve.

3-D Histomorphometric Reconstruction of the ONH

The ONH and peripapillary sclera of each eye were trephined (3-mm-diameter), embedded in paraffin, mounted to a microtome (RM2165; Leica, Wetzlar, Germany) and serial sectioned at 1.5 μm thickness from the vitreous surface through the optic nerve head into the orbital optic nerve (Burgoyne et al., 2004). After each section was cut, the block surface was stained with a 1:1 (v/v) mixture of Ponceau S and acid fuchsin stains, then imaged at a resolution of 1.5 × 1.5 μm per pixel using a custom device (Burgoyne et al., 2004). For each ONH 275 to 501 serial digital transverse section images were thus generated, aligned and stacked into a digital 3-D reconstruction (Burgoyne et al., 2004; Downs et al., 2007; Yang et al., 2007a; Yang et al., 2009a; Yang et al., 2007b; Yang et al., 2011a).

3-D Delineation of the Rat ONH and Peripapillary Scleral Landmark Points

Each 3-D ONH reconstruction was loaded into our custom Multiview 3-D visualization and delineation software (based on the Visualization Toolkit [VTK], Clifton Park, NY) (Burgoyne et al., 2004; Downs et al., 2007; Morrison et al., 1999; Yang et al., 2007a; Yang et al., 2009a; Yang et al., 2007b). A delineator assigned the approximate center of the optic nerve (Supplemental Figure 3) as the center of rotation, through which, forty, 7-voxel thick, digital radial sagittal slices of the digital 3-D reconstruction were serially served at 4.5º intervals for delineation. Because visualization of Bruch's Membrane (BM), Bruch's Membrane Opening (BMO) and several deep ONH landmarks was most consistent within Green channel as opposed to white light section images, delineation was carried out within green channel digital section images for each study eye. Four landmark surfaces and three pairs of neurovascular canal landmark points (one point on each side of the canal) were delineated within each digital section image (Supplemental Figure 3). The landmark surfaces were: (1) BM; (2) the anterior and (3) posterior surfaces of peripapillary sclera; and (4) the outer optic nerve boundaries extending on both sides of the nerve from BMO,

through the neurovascular scleral canal and along the pia mater to the posterior edge of the reconstruction. The landmark points were BMO, the anterior scleral canal opening (ASCO) and the posterior scleral canal opening (PSCO).

Masked Delineation Strategy

Both eyes of each rat were delineated by a single delineator who was masked to the treatment status of each eye. Final delineations were checked for accuracy by two experienced observers (HY and CFB) masked as to the treatment condition of each eye.

Delineation Reproducibility Study

Both the Control and EG eye of each animal were delineated by a single delineator (MP). Upon completion of the initial delineation of each eye, the marks were reviewed by 2 authors (CFB and HY) to expand our understanding of the anatomy and to reach agreement on the anatomic landmarks of greatest interest. Both eyes of three animals were then delineated on two subsequent occasions by the same delineator (MP), at least 2 weeks apart, to assess intra-delineator variability. The intraclass-Correlation Coefficient (ICC) (see statistical analysis, below) for all reported parameters were calculated (Rosner, 2011).

Parameterization and Quantification

For each 3-D ONH reconstruction, a plane satisfying a least-squares error restraint was fit to the 80 BMO points (Pazos et al., 2015), creating a BMO reference plane which served as the reference plane for a series of subsequent measurements (Supplemental Figure 4) and the base for the second peripheral anterior scleral reference plane (Supplemental Figure 6). The following parameters have been previously described (Pazos et al., 2015) and are illustrated in Supplemental Figures 4–7: BMO and the neurovascular canal parameters: *ASCO and PSCO Areas, Radii and Depths,* Horizontal/Vertical (H/V) Diameter Ratios for BMO, ASCO and PSCO; Optic Nerve cross-sectional parameters: Optic Nerve cross sectional area, radii and shape (H/V diameter ratios) at the level of ASCO (*ON-ASCO*) and PSCO (*ON-PSCO*) as well as the *Optic Nerve Volume*; Scleral and Choroidal Parameters: *Scleral Sling Depth, Scleral Depth, Scleral Thickness and Choroidal Thickness*. In addition, to assess preferential displacement of the nerve within the neurovascular canal of the EG eyes, two new parameters measuring the distance between the neurovascular scleral canal wall and the contained optic nerve (the optic nerve gap distance) were calculated within all 80 radial locations: 1) the ASCO to ON-ASCO distance *(ASCO ON-ASCO Distance);* and 2) the PSCO to ON-PSCO distance (*PSCO ON-PSCO Distance)* (See Figure 2 and Supplemental Figure 11, (respectively) for diagrams.

Statistical Analysis

EG versus Control eye global data were compared using a paired, two-sided student T-test with significance defined to occur at $p<0.0022$ to adjust for multiple (n=23) comparisons (Guo and Yuan, 2015). For the subset of parameters with multiple values per eye, overall (experiment-wide) EG eye effects were assessed within each region using a linear mixed effects model, accounting for multiple data points per eye and two eyes per rat (significance defined at $p<0.0125$, to adjust for 4 regional comparisons per parameter). An exponential

spatial correlation structure was assumed within each eye, based on the distances between delineated points. EG vs Control eye comparisons for each animal globally (significance defined at $p<0.005$,13 comparisons per rat) and by each quadrant (significance defined at $p<0.0001$, 13 comparisons per quadrant) were carried out using generalized least squares models assuming exponential spatial correlation structure. Within the reproducibility study, the ICC was calculated from one-way ANOVA. Correlation between the magnitude of global EG eye change in the area and volume optic nerve parameters (ASCO area, PSCO area, ON-ASCO area, ON-PSCO area and ON Volume) and the orbital optic nerve injury scale was assessed for statistical significance using Pearson's correlation coefficient ($p<0.05$ without adjustment due to the small number of purposeful comparisons). Analysis was carried out either in R (the R Foundation for Statistical Computing, Vienna, Austria) or Microsoft Excel (Microsoft, Redmond, WA, USA).

Results

Animal and Eye Data (Table 2)

Both the EG and the Control eyes of eight brown male Norway rats (aged from 9.5 to 10.5 months) were studied. A detailed description of the 8 Control eyes is contained within our previous report (Pazos et al., 2015). Eye-specific mean IOP in the Control eyes ranged from 28.3 to 28.5 mmHg. Eye-specific mean IOP in the EG eyes ranged from 28.3 to 34.6 mmHg, with *Mean IOP Differences* ranging from 0.4 to 6.6 mmHg and *Peak IOPs* ranging from 36 to 45.8 mmHg. The *mean optic nerve damage grade* for all 8 Control eyes was 1.0 (no detectable damage) and ranged from 1.22 (Rat 1) to 3.28 (Rat 8) in the EG eyes. For this and the previous normal Control eye report (Pazos et al., 2015) study animals were numbered 1–8 based on the magnitude of each animal's EG eye *optic nerve damage grade*. Several parameters could not be calculated for the EG eye of Animal 6 due to poor visualization of the outer scleral canal and peripapillary sclera.

Delineation Reproducibility

Reproducibility was excellent (ICC values greater than 0.75) or fair to good (ICC 0.49–0.75) for all parameters included in this study (Supplemental Table 1).

Overall and Animal Specific Global and Regional Parameter Change

Overall global values for each parameter by treatment group are reported in Table 3. Animal-specific, global parameter change is reported in Supplemental Table 2 and its frequency (among the 8 EG eyes) and direction are summarized for each parameter in Table 4. Overall regional values for each parameter by treatment group are reported in Table 5. The frequency of animal-specific, EG eye regional change is summarized for each parameter in Table 6.

Neurovascular Canal—EG versus Control eye plots of BMO, ASCO and PSCO are shown for each animal in Figure 1 and Supplemental Figures 8–10. Overall mean *ASCO Area* was 24% larger ($p<.0016$) and mean *ASCO radius* was 11% larger ($p<.0016$) in the EG compared to the Control eyes (Table 3). Animal-specific EG eye values were significantly larger than Control eyes for *BMO Radius* in 5 animals (ranging from 3 to 10%) (Figure 1

and Table 4), *ASCO Radius* in 7 animals (ranging from 8 to 21% (Figures 1–2, and Table 4), and *PSCO Radius in* 6 of the 7 EG eyes with *PSCO Radius* measurements (ranging from 5 to 21%).

Within the overall regional analysis (Table 5), *ASCO Radius* demonstrated significantly larger EG vs Control eye values within the superior and temporal quadrants ($p<0.0125$). Animal-specific EG vs Control eye values for *ASCO Radius* were larger within 7 animals and smaller in the 8th within the superior quadrant, and larger in 5 animals temporally, nasally and inferiorly. EG versus Control eye values for *PSCO Radius* were larger in 5 animals within the superior, nasal and temporal quadrants.

Optic Nerve—Among all statistically significant EG versus Control Eye differences, optic nerve size differences were greatest in magnitude and occurred most consistently among the 8 EG eyes. EG versus Control eye plots of ON-ASCO relative to ASCO (Figure 2), ON-ASCO alone (Figure 3) and ON-PSCO alone (Figure 4) demonstrate larger EG eye optic nerves at both openings. Overall mean *ON-ASCO Area* was 32% larger and mean *ON-ASCO radius* was 16% larger in the EG compared to the Control eyes ($p<.0021$ and $p<.0012$, respectively). Overall mean *ON-ASCO H/V Diameter Ratio* was 22.5% smaller in the EG compared to the Control eyes, ($p<0.001$) suggesting that EG eye optic nerve expansion was greater within the vertical compared to the horizontal axis.

Animal-specific EG eye values were significantly larger than Control eye values for: *ON-ASCO Radius* within 7 animals (ranging from 11 to 30%, $p<0.005$, Figures 2 and 3) and *ON-PSCO Radius* in 6 out of the 7 animals in which it could be measured (ranging from 8 to 41%, $p<0.005$, Figure 4 and Supplemental Figure 11). Within the overall regional analysis, (Table 5), *ON-ASCO Radius* and *ON-PSCO Radius* demonstrated significantly larger EG versus Control eye values within the superior region. EG eye values were significantly larger than Control eyes for *ON-ASCO Radius* in all 8 animals within the superior and inferior quadrants (Table 6). EG eye values were significantly larger than Control eye values for *ON-PSCO Radius* in 6 animals within the superior and 5 animals within the inferior quadrant (Table 6).

Optic Nerve to Scleral Canal Gap Distance (Figure 2)—Animal-specific EG eye values were significantly larger than Control eye values for *ASCO-ON-ASCO in 4 animals* ranging from 18 to 26% and significantly smaller (by 13%) in a fifth animal (Table 4). EG eye values were significantly larger than Control eye values for *ASCO-ON-ASCO* in 5 animals superiorly, significantly smaller in 5 animals inferiorly and significantly larger in 4 animals nasally (Table 6).

Peripapillary Sclera and Choroid—Animal-specific EG eye values for *Scleral Depth* were significantly larger than Control eyes in 4 animals and smaller than the Control eye in a 5th animal (Table 4). All 8 animals demonstrated significant EG versus Control eye differences in *Choroidal Thickness* with 6 animals demonstrating smaller EG eye values (ranging from −29 to −7%) and 2 animals demonstrating larger EG eye values (ranging from 8–32%). *Choroidal Thickness* demonstrated the most frequent animal-specific, regional EG

versus control eye differences with EG eye values smaller than Control eyes in 6 animals superiorly, 5 animals inferiorly, and 4 animals nasally and temporally.

Correlation with orbital optic nerve axon degeneration

ON-PSCO Area expansion was significantly correlated to EG eye *optic nerve injury grade* (R=0.768; p=0.042) among the 7 EG eyes for which there was ON-PSCO data (Figure 5).

Discussion

This study 3D histomorphometrically characterizes early ONH neural and connective tissue change in the hypertonic rat model of unilateral EG. Our principle findings are as follows. First, the connective tissue openings that define the neurovascular canal of the rat ONH, (BMO, ASCO and PSCO), each expand early in EG. Second, among all forms of EG eye change, optic nerve expansion within the scleral canal was greatest in magnitude, occurred most frequently among the 8 EG eyes, and was preferential to the superior and inferior quadrants. Third, the magnitude of optic nerve expansion correlated to the post-mortem optic nerve axon injury grade.

EG eye expansions of the neurovascular canal and contained optic nerve (Figure 6) were present in all 8 animals. Five of 8 EG eyes demonstrated *BMO radius* expansion, 7 of 8 EG eyes demonstrated *ASCO radius* expansion and *PSCO radius* expansion was detected in 6 of the 7 EG eyes in which it could be measured. Chauhan et al (Chauhan et al., 2002), using the hypertonic saline model, was the first to document sequential and progressive ONH surface “cupping” as well as probable BMO and scleral canal expansion by in vivo confocal scanning laser tomography (CSLT) in the rat EG model. However, CSLT alterations in the ONH neural canal opening were only detected after significant elevations of IOP and in association with loss of over 55% of the axons. In that study, it is not clear if BMO or the ASCO was being measured within the CSLT data sets because the nature of what is seen as the “disc margin” in clinical photographs and CSLT images of rat eyes has not yet been determined(Reis et al., 2012a; Reis et al., 2012b; Strouthidis et al., 2010; Strouthidis et al., 2009). Guo et al, (Guo et al., 2005) using en-face in-vivo Optical Coherence Tomography (OCT), reported progressive expansion of the optic disc area and a progressive ASCO expansion in 18 Dark Agouti EG rats. However, in their study, OCT visualization of BM, BMO, the anterior scleral surface and the ASCO were not clearly documented relative to one another.

Our post-mortem data clarify these findings by detecting neurovascular canal expansion at the level of BMO and the sclera (ASCO and PSCO) early in the optic neuropathy of chronic IOP elevation in the rat eye. We observed significant changes in ASCO in EG eyes with optic nerve injury grades of 2 through 3.28 which equate to estimated axonal loss from 15 to 34%-using the Morrison conversion scale (Jia et al., 2000; Morrison et al., 2005).

Our data further suggest radial optic nerve expansion within the neurovascular scleral canal and suggest the magnitude of expansion correlates to orbital optic nerve injury. These findings are important because the detection of longitudinal change in the diameter of the optic nerve within the neurovascular scleral canal may become an achievable OCT imaging

target as this technology is applied to the rodent eye (Fortune et al., 2011; Guo and Yuan, 2015; Nagata et al., 2009; Zhang et al., 2011). EG eyes also demonstrated significantly larger increases in *ON-ASCO* and *ON-PSCO Radius* in the superior and inferior regions, significant *ON-ASCO H/V diameter ratio* reduction and animal-specific changes in the *ASCO-ON*-ASCO gap distance that most frequently occurred in the superior and inferior quadrants. Taken together these findings suggest preferential optic nerve expansion within the vertical compared to the horizontal axes. These findings may be manifestations of, or contribute, to the mechanisms which underlie, previously reported, preferential superior susceptibility to ONH axonal damage in the rat eye (Dai et al., 2012; Huang and Knighton, 2009; Li et al., 2015; Morrison, 2005; Morrison et al., 1997; WoldeMussie et al., 2001),

EG eye optic nerve expansion may be a manifestation of edema, cell proliferation, remodeling and/or synthesis of “laminar-like” connective tissue (Johnson et al., 1996). In a separate study of rat early EG eyes, swollen axons have been noted within the ONH, filled with vesicular material consistent with both axon transport obstruction and axonal degeneration (Morrison et al., 1997). More recently, genomic studies have demonstrated mRNA alterations compatible with cell proliferation pathways at the same stage of damage (Howell et al., 2011; Johnson et al., 2011; Johnson et al., 2007). We have previously reported thickening of the lamina cribrosa and profound connective tissue remodeling at a similar early stage of monkey EG (Burgoyne, 2015b; Burgoyne et al., 2014; Yang et al., 2007b; Yang et al., 2011b) (Stowell C, et al. *IOVS* 2014;55:ARVO E-Abstract 5034).

In the primate, the peripapillary sclera and scleral canal wall connective tissues are thought to govern the distribution of IOP-related stress within the lamina cribrosa connective tissues (Burgoyne and Downs, 2008; Sigal, 2009; Sigal et al., 2009a, b). The question of how the sclera transfers load to the rodent retinal ganglion cell axons and the astrocytes that span the nerve within the canal is of substantial biomechanical interest. Two recent papers have described the relationship between the radially arrayed, rat optic nerve head astrocytes, the optic nerve sheath (a continuation of the pia that merges with Bruch’s Membrane at its opening – see Supplemental Figures 2–4) and the vascular plexus that surrounds the nerve within the neurovascular canal, effectively isolating it from the sclera (Dai et al., 2012; Li et al., 2015).

In the first of these articles (Dai et al., 2012), Dai and colleagues described a radial array of “fortified” astrocytes in the normal rat ONH, and early disinsertion of the superior astrocyte footplates from the pial sheath with subsequent loss of the astrocytes and eventual axon loss following 1 week of chronic IOP elevation. Their description of the vascular plexus that surrounds the optic nerve, (which is poorly visualized within our reconstructions due to its heavy pigmentation) suggests that it contains dense connective tissue septa. We suggest that if these septa directly or indirectly span the plexus to link the sheath and the sclera, they may be the means by which the sclera transfers IOP-related load to the radial ONH astrocytic array. It is possible that the inferior shift of the nerve within the canal demonstrated in 5 of the 8 EG eyes in this report, reflects damage to the superior vascular plexus connective tissue septa that both explains this shift and either contributes to or results from the processes that damage the underlying astrocyte footplates.

Previous studies in the monkey unilateral EG model (Burgoyne et al., 2004; Downs et al., 2007; Yang et al., 2007a; Yang et al., 2007b) have reported only small *BMO area* increases and only in a small subset of early EG eyes (Burgoyne et al., 2004; Downs et al., 2007; Yang et al., 2007a; Yang et al., 2007b). In the present study, global *BMO radius* expansion was present in 5 of the 8 animals and regional expansion was present in a subset of eyes. While the *cumulative IOP insults* to the rat and monkey BMO connective tissues should not be directly compared, the frequency of BMO expansion in early rat EG suggests that the rat BM connective tissues immediately adjacent to BMO may demonstrate less structural stiffness than those of the monkey either due to being less thick or more compliant or both.

The choroid was thinner in the EG (compared to the Control) eyes of 6 animals and thicker in 2 animals. Between-eye differences in choroidal thickness in our study eyes should be interpreted carefully because the study was not designed to test hypotheses about choroidal thickness and IOP was not manometrically controlled at the same level in the Control and EG eyes at the time of perfusion. The peripapillary choroid likely plays an important role in the rat ONH blood supply since it is continuous with the vascular plexus surrounding the optic nerve within the neurovascular scleral canal. In vivo, longitudinal choroidal thickness measurements at manometrically controlled pressures by OCT(Pierru et al., 2014; Wang and Zhang, 2014; Yiu et al., 2014) are required to detect longitudinal choroidal thickness changes in the rat EG models. Separate from thickness, choroidal blood flow measurements within these vessels may be soon within the reach of a variety of OCT angiographic techniques(Baumann et al., 2011; Zhi et al., 2011; Zhi et al., 2012; Zotter et al., 2011).

Outward bowing of the peripapillary sclera was indirectly assessed in this study using two parameters - *Scleral Depth* and *BMO Depth* (Supplemental Figure 3) both of which measured relative to a peripheral scleral reference plane. Outward bowing of the peripapillary sclera relative to this more peripheral reference plane would be expected to manifest as an increase in both parameters if no other effects were present. *Scleral Depth* was increased in 4 and decreased in 1 EG eye, respectively. *BMO Depth* was significantly increased in 5 and decreased in 2 EG eyes. Direct longitudinal detection of posterior bowing of the peripapillary sclera by in-vivo SDOCT or MRI imaging in eyes carried to more advanced stages of IOP insult is required to confirm the significance of these findings (He et al., 2014; Heickell et al., 2001; Strouthidis et al., 2011a).

The limitations of our method of 3-D reconstruction have been previously discussed (Burgoyne et al., 2004; Pazos et al., 2015) and include: (1) anterior-to-posterior resolution limited to 1.5 μm; (2) hand application of the stain to the block face using a cotton-tipped swab providing the potential for substantial staining variation between section images; (3) tissue shrinkage effects (both from fixation and embedding) which may be unique to the rat eye. While comparisons to our nonhuman primate (Burgoyne et al., 2004; Downs et al., 2007; Yang et al., 2007a; Yang et al., 2007b; Yang et al., 2009b) publications may be similar (since fixation and post-tissue processing is similar), comparisons to other post-mortem or in-vivo measurements may be profoundly affected by these differences.

We intended to study rats with early damage which is why all animals were sacrificed after 4 weeks of IOP elevation. The statistical significance of many of the changes is likely

dependent on this choice. While the ONH are “early” in terms of time (4 weeks since injection), the percent axon loss in the EG eyes of this study, (as estimated by the correlation between axon counts to axon damage injury grade correlations) (Morrison et al., 2005), were *<5%, ≈10%, ≈18%, <20%, <22%, <35%, <35%, and ≈35%, respectively.* These data suggest that the majority of EG eyes in this study were at an early to moderate stage of axon loss. Determination of the earliest ONH alterations in the rat EG model will be the subject of future reports. Characterization of maximum physiologic between eye differences (Yang et al., 2009a) (using bilateral normal animals) is ultimately required to be certain that the early EG eye differences we report exceed between eye-differences within bilaterally normal animals. Generalization of our findings to naïve normal eyes of all ages, strain and lighting conditions should not be assumed.

The animals in this study were sacrificed using sodium nitroprusside which is a potent vasodilator that is commonly given to improve the removal of blood from the ONH vasculature during perfusion fixation. While it is unlikely that our finding of EG eye scleral canal expansion was influenced by vasodilation, it is conceivable that the optic nerve blood vessels in the EG eyes were preferentially influenced by the nitroprusside and a portion or all of the optic nerve expansion was on this basis. Certainly, as deep optic nerve head imaging improves in the rat experimental glaucoma models, longitudinal detection of scleral canal expansion as well as optic nerve expansion within the scleral canal should be confirmed using these techniques. However, we do not believe that preferential optic nerve swelling in the EG eye is the most likely explanation for our optic nerve findings for the following reasons. First, we would expect that the peri-neural vascular plexus would dilate more than the smaller vessels in the optic nerve and this would have the net effect of compressing rather than expanding the nerve within the scleral canal. Second, the genomic studies mentioned above, have demonstrated significant increases in DNA content and mRNA alterations compatible with cell proliferation pathways and inflammation at the same stage of damage (Howell et al., 2011; Johnson et al., 2011; Johnson et al., 2007). We believe that these processes, alone, likely underlie optic nerve enlargement in the EG eye.

Finally, to date, there have been no rigorous descriptions of what constitutes a “*glaucomatous”* optic neuropathy in the rodent eye. In the monkey, we have argued that ONH surface “cupping” that does not include ONH connective tissue deformation and remodeling is a non-specific feature of all forms of RGC axonal injury and is not specific to chronic IOP elevation (Burgoyne, 2015a). From our findings in monkeys (Burgoyne, 2015b; He et al., 2014; Strouthidis et al., 2011b) we have argued that the same features of the neuropathy should be present in human eyes and we are currently using OCT ONH imaging to describe these phenomena in glaucoma patients (Ren et al., 2014).

We propose that the rat ONH neural and connective tissue alterations described herein are core components of the neuropathy that occurs 4 weeks after the onset of chronic moderate experimental IOP elevation in the rat eye. Their presence should be sought and confirmed in all experimental models of “glaucomatous” optic neuropathy in the rat eye whether due to spontaneous (Goldblum and Mittag, 2002) or experimental chronic IOP elevation (Chauhan et al., 2002; Morrison et al., 2008; Morrison et al., 1997), ischemia (Naskar et al., 2002),

endothelin (Chauhan et al., 2004; Murphy et al., 2010; Prasanna et al., 2011), or immune system manipulation (Joachim et al., 2013; Tezel and Wax, 2004; Wax et al., 2008).

Because there are, at present, no experimental models for the induction of a glaucomatous optic neuropathy in any species that do not depend upon chronic IOP elevation, such a model remains an important experimental target for glaucoma research. We propose that our findings should serve as phenotypic benchmarks for all future rat models of glaucomatous ONH injury that do (Chauhan et al., 2002; Goldblum and Mittag, 2002; Morrison, 2005; Morrison et al., 2008; Morrison et al., 1997; WoldeMussie et al., 2001) and do not (Chauhan et al., 2004; Naskar et al., 2002; Prasanna et al., 2011; Tezel and Wax, 2004; Tseng et al., 2015; Votruba et al., 2003; Wax et al., 2008; WoldeMussie et al., 2001) involve spontaneous or experimental IOP elevation.

In summary, we have performed the first 3D histomorphometric study of early alterations to the rat ONH following chronic experimental IOP elevation. Our findings suggest that radial expansion of the ONH connective tissue openings in Bruch's Membrane and the sclera, as suggested by previous studies (Chauhan et al., 2002; Guo et al., 2005), accompanied by preferential superior and inferior radial expansion of the optic nerve within the scleral canal are early components of the optic neuropathy of chronic experimental IOP elevation in the rat eye.

Supplementary Material

Refer to Web version on PubMed Central for supplementary material.

Acknowledgments

The authors gratefully acknowledge the following individuals for their assistance with this study. Juan Reynaud for his assistance with improving the visibility of the rat ONH anatomy within the green channel and providing software for volumetric and thickness quantification. Galen Williams for his assistance with serial sectioning the tissues. Joanne Couchman for her assistance with manuscript preparation.

Supported in part by NIH grants R01EY011610 (CFB), R01EY10145 (JCM) and R01EY16866 (ECJ)) from the National Eye Institute, National Institutes of Health, Bethesda, Maryland; The Legacy Good Samaritan Foundation, Portland, Oregon; the Sears Trust for Biomedical Research, Mexico, Missouri; the Alcon Research Institute, Fort Worth, Texas; and an unrestricted grant from Research to Prevent Blindness.

References

Baumann B, et al. Total retinal blood flow measurement with ultrahigh speed swept source/Fourier domain OCT. Biomed Opt Express. 2011; 2:1539–1552. [PubMed: 21698017]

Burgoyne C. The Morphological Difference Between Glaucoma and Other Optic Neuropathies. J Neuroophthalmol. 2015a; 35(Suppl 1):S8–S21. [PubMed: 26274837]

Burgoyne CF. The non-human primate experimental glaucoma model. Exp Eye Res. 2015b First published on Jun 9, 2015b. 10.1016/j.exer.2015.06.005

Burgoyne CF, Downs JC. Premise and prediction-how optic nerve head biomechanics underlies the susceptibility and clinical behavior of the aged optic nerve head. J Glaucoma. 2008; 17:318–328. [PubMed: 18552618]

Burgoyne CF, et al. Three-dimensional reconstruction of normal and early glaucoma monkey optic nerve head connective tissues. Invest Ophthalmol Vis Sci. 2004; 45:4388–4399. [PubMed: 15557447]

Burgoyne CF, et al. Non-Human Primate (NHP) Optic Nerve Head (ONH) Proteomic Change In Early Experimental Glaucoma (EEG). ARVO Meeting Abstracts. 2014; 55 ARVO Abstract# 4555.

Cepurna WO, et al. Age related optic nerve axonal loss in adult Brown Norway rats. Exp Eye Res. 2005; 80:877–884. [PubMed: 15939045]

Chauhan BC, et al. Model of endothelin-1-induced chronic optic neuropathy in rat. Invest Ophthalmol Vis Sci. 2004; 45:144–152. [PubMed: 14691166]

Chauhan BC, et al. Effect of intraocular pressure on optic disc topography, electroretinography, and axonal loss in a chronic pressure-induced rat model of optic nerve damage. Invest Ophthalmol Vis Sci. 2002; 43:2969–2976. [PubMed: 12202517]

Crowston JG, et al. An acute intraocular pressure challenge to assess retinal ganglion cell injury and recovery in the mouse. Exp Eye Res. 2015 First published on Mar 7, 2015. 10.1016/j.exer.2015.03.006

Dai C, et al. Structural basis of glaucoma: the fortified astrocytes of the optic nerve head are the target of raised intraocular pressure. Glia. 2012; 60:13–28. [PubMed: 21948238]

Downs JC, et al. Three-dimensional histomorphometry of the normal and early glaucomatous monkey optic nerve head: neural canal and subarachnoid space architecture. Invest Ophthalmol Vis Sci. 2007; 48:3195–3208. [PubMed: 17591889]

Fernandes KA, et al. Using genetic mouse models to gain insight into glaucoma: Past results and future possibilities. Exp Eye Res. 2015 First published on Jun 24, 2015. 10.1016/j.exer.2015.06.019

Fortune B, et al. Deformation of the rodent optic nerve head and peripapillary structures during acute intraocular pressure elevation. Invest Ophthalmol Vis Sci. 2011; 52:6651–6661. [PubMed: 21730343]

Goldblum D, Mittag T. Prospects for relevant glaucoma models with retinal ganglion cell damage in the rodent eye. Vision Res. 2002; 42:471–478. [PubMed: 11853763]

Guo B, Yuan Y. A comparative review of methods for comparing means using partially paired data. Stat Methods Med Res. 2015 First published on Apr 1, 2015. 10.1177/0962280215577111

Guo L, et al. En face optical coherence tomography: a new method to analyse structural changes of the optic nerve head in rat glaucoma. Br J Ophthalmol. 2005; 89:1210–1216. [PubMed: 16113384]

He L, et al. Longitudinal detection of optic nerve head changes by spectral domain optical coherence tomography in early experimental glaucoma. Invest Ophthalmol Vis Sci. 2014; 55:574–586. [PubMed: 24255047]

Heickell AG, et al. Optic disc surface compliance testing using confocal scanning laser tomography in the normal monkey eye. J Glaucoma. 2001; 10:369–382. [PubMed: 11711833]

Hernandez MR, et al. Changes in the extracellular matrix of the human optic nerve head in primary open-angle glaucoma. Am J Ophthalmol. 1990; 109:180–188. [PubMed: 2405683]

Howell GR, et al. Molecular clustering identifies complement and endothelin induction as early events in a mouse model of glaucoma. J Clin Invest. 2011; 121:1429–1444. [PubMed: 21383504]

Huang XR, Knighton RW. Altered F-actin distribution in retinal nerve fiber layer of a rat model of glaucoma. Exp Eye Res. 2009; 88:1107–1114. [PubMed: 19450448]

Jia L, et al. Patterns of intraocular pressure elevation after aqueous humor outflow obstruction in rats. Invest Ophthalmol Vis Sci. 2000; 41:1380–1385. [PubMed: 10798653]

Joachim SC, et al. Immune response against ocular tissues after immunization with optic nerve antigens in a model of autoimmune glaucoma. Mol Vis. 2013; 19:1804–1814. [PubMed: 23946635]

Johnson EC, et al. Cell proliferation and interleukin-6-type cytokine signaling are implicated by gene expression responses in early optic nerve head injury in rat glaucoma. Invest Ophthalmol Vis Sci. 2011; 52:504–518. [PubMed: 20847120]

Johnson EC, et al. Global Changes in Optic Nerve Head Gene Expression after Exposure to Elevated Intraocular Pressure in a Rat Glaucoma Model. Invest Ophthalmol Vis Sci. 2007; 48:3161–3177. [PubMed: 17591886]

Johnson EC, et al. The effect of chronically elevated intraocular pressure on the rat optic nerve head extracellular matrix. Exp Eye Res. 1996; 62:663–674. [PubMed: 8983948]

Kong YX, et al. Functional changes in the retina during and after acute intraocular pressure elevation in mice. Invest Ophthalmol Vis Sci. 2009; 50:5732–5740. [PubMed: 19643960]

Li Y, et al. An energy theory of glaucoma. Glia. 2015; 63:1537–1552. [PubMed: 25808326]

Morgan JE, Tribble JR. Microbead models in glaucoma. Exp Eye Res. 2015 First published on Jun 24, 2015. 10.1016/j.exer.2015.06.020

Morrison J, et al. Structure and composition of the rodent lamina cribrosa. Exp Eye Res. 1995; 60:127–135. [PubMed: 7781741]

Morrison JC. Elevated intraocular pressure and optic nerve injury models in the rat. J Glaucoma. 2005; 14:315–317. [PubMed: 15990616]

Morrison JC, et al. Modeling glaucoma in rats by sclerosing aqueous outflow pathways to elevate intraocular pressure. Exp Eye Res. 2015 First published on May 21, 2015. 10.1016/j.exer.2015.05.012

Morrison JC, et al. Pathophysiology of human glaucomatous optic nerve damage: insights from rodent models of glaucoma. Exp Eye Res. 2011; 93:156–164. [PubMed: 20708000]

Morrison JC, et al. Optic nerve head extracellular matrix in primary optic atrophy and experimental glaucoma. Arch Ophthalmol. 1990; 108:1020–1024. [PubMed: 2369339]

Morrison JC, et al. Rat models for glaucoma research. Prog Brain Res. 2008; 173:285–301. [PubMed: 18929117]

Morrison JC, et al. Understanding mechanisms of pressure-induced optic nerve damage. Prog Retin Eye Res. 2005; 24:217–240. [PubMed: 15610974]

Morrison JC, et al. Microvasculature of the rat optic nerve head. Invest Ophthalmol Vis Sci. 1999; 40:1702–1709. [PubMed: 10393039]

Morrison JC, et al. A rat model of chronic pressure-induced optic nerve damage. Exp Eye Res. 1997; 64:85–96. [PubMed: 9093024]

Morrison JC, et al. Glaucoma drops control intraocular pressure and protect optic nerves in a rat model of glaucoma. Invest Ophthalmol Vis Sci. 1998; 39:526–531. [PubMed: 9501862]

Murphy JA, et al. The role of endothelin-1 and its receptors in optic nerve head astrocyte proliferation. Br J Ophthalmol. 2010; 94:1233–1238. [PubMed: 20494907]

Nagata A, et al. In vivo quantitative evaluation of the rat retinal nerve fiber layer with optical coherence tomography. Invest Ophthalmol Vis Sci. 2009; 50:2809–2815. [PubMed: 19182247]

Naskar R, et al. Detection of early neuron degeneration and accompanying microglial responses in the retina of a rat model of glaucoma. Invest Ophthalmol Vis Sci. 2002; 43:2962–2968. [PubMed: 12202516]

Overby DR, Clark AF. Animal models of glucocorticoid-induced glaucoma. Exp Eye Res. 2015 First published on Jun 4, 2015. 10.1016/j.exer.2015.06.002

Pang IH, et al. Elevation of intraocular pressure in rodents using viral vectors targeting the trabecular meshwork. Exp Eye Res. 2015 First published on May 26, 2015. 10.1016/j.exer.2015.04.003

Pang IH, et al. Acute effects of glaucoma medications on rat intraocular pressure. Exp Eye Res. 2005; 80:207–214. [PubMed: 15670799]

Pazos M, et al. Rat optic nerve head anatomy within 3D histomorphometric reconstructions of normal control eyes. Exp Eye Res. 2015; 139:1–12. [PubMed: 26021973]

Pierru A, et al. Measurement of subfoveal choroidal thickness after cataract surgery in enhanced depth imaging optical coherence tomography. Invest Ophthalmol Vis Sci. 2014; 55:4967–4974. [PubMed: 25052991]

Prasanna G, et al. Endothelin, astrocytes and glaucoma. Exp Eye Res. 2011; 93:170–177. [PubMed: 20849847]

Reis AS, et al. Influence of clinically invisible, but optical coherence tomography detected, optic disc margin anatomy on neuroretinal rim evaluation. Invest Ophthalmol Vis Sci. 2012a; 53:1852–1860. [PubMed: 22410561]

Reis AS, et al. Optic disc margin anatomy in patients with glaucoma and normal controls with spectral domain optical coherence tomography. Ophthalmology. 2012b; 119:738–747. [PubMed: 22222150]

Ren R, et al. Anterior lamina cribrosa surface depth, age, and visual field sensitivity in the Portland Progression Project. Invest Ophthalmol Vis Sci. 2014; 55:1531–1539. [PubMed: 24474264]

Rosner, B. 12.9. The Intraclass Correlation Coefficient, Fundamentals of Biostatistics. 7. Harvard University. Brooks/Cole Cengage Learning; Boston, MA: 2011. p. 569

Schlamp CL, et al. Progressive ganglion cell loss and optic nerve degeneration in DBA/2J mice is variable and asymmetric. BMC Neurosci. 2006; 7:66. [PubMed: 17018142]

Sigal IA. Interactions between geometry and mechanical properties on the optic nerve head. Invest Ophthalmol Vis Sci. 2009; 50:2785–2795. [PubMed: 19168906]

Sigal IA, et al. Modeling individual-specific human optic nerve head biomechanics. Part I: IOP-induced deformations and influence of geometry. Biomech Model Mechanobiol. 2009a; 8:85–98. [PubMed: 18309526]

Sigal IA, et al. Modeling individual-specific human optic nerve head biomechanics. Part II: influence of material properties. Biomech Model Mechanobiol. 2009b; 8:99–109. [PubMed: 18301933]

Strouthidis NG, et al. Effect of acute intraocular pressure elevation on the monkey optic nerve head as detected by spectral domain optical coherence tomography. Invest Ophthalmol Vis Sci. 2011a; 52:9431–9437. [PubMed: 22058335]

Strouthidis NG, et al. Longitudinal change detected by spectral domain optical coherence tomography in the optic nerve head and peripapillary retina in experimental glaucoma. Invest Ophthalmol Vis Sci. 2011b; 52:1206–1219. [PubMed: 21217108]

Strouthidis NG, et al. A comparison of optic nerve head morphology viewed by spectral domain optical coherence tomography and by serial histology. Invest Ophthalmol Vis Sci. 2010; 51:1464–1474. [PubMed: 19875649]

Strouthidis NG, et al. Comparison of clinical and spectral domain optical coherence tomography optic disc margin anatomy. Invest Ophthalmol Vis Sci. 2009; 50:4709–4718. [PubMed: 19443718]

Sugiyama K, et al. Optic nerve and peripapillary choroidal microvasculature of the rat eye. Invest Ophthalmol Vis Sci. 1999; 40:3084–3090. [PubMed: 10586928]

Tezel G, Wax MB. The immune system and glaucoma. Curr Opin Ophthalmol. 2004; 15:80–84. [PubMed: 15021215]

Tseng HC, et al. Visual impairment in an optineurin mouse model of primary open-angle glaucoma. Neurobiol Aging. 2015; 36:2201–2212. [PubMed: 25818176]

Votruba M, et al. Optic disc morphology of patients with OPA1 autosomal dominant optic atrophy. Br J Ophthalmol. 2003; 87:48–53. [PubMed: 12488262]

Wang W, Zhang X. Choroidal thickness and primary open-angle glaucoma: a cross-sectional study and meta-analysis. Invest Ophthalmol Vis Sci. 2014; 55:6007–6014. [PubMed: 25168904]

Wax MB, et al. Induced autoimmunity to heat shock proteins elicits glaucomatous loss of retinal ganglion cell neurons via activated T-cell-derived fas-ligand. J Neurosci. 2008; 28:12085–12096. [PubMed: 19005073]

WoldeMussie E, et al. Neuroprotection of retinal ganglion cells by brimonidine in rats with laser-induced chronic ocular hypertension. Invest Ophthalmol Vis Sci. 2001; 42:2849–2855. [PubMed: 11687528]

Yang H, et al. 3-D histomorphometry of the normal and early glaucomatous monkey optic nerve head: prelaminar neural tissues and cupping. Invest Ophthalmol Vis Sci. 2007a; 48:5068–5084. [PubMed: 17962459]

Yang H, et al. Physiologic intereye differences in monkey optic nerve head architecture and their relation to changes in early experimental glaucoma. Invest Ophthalmol Vis Sci. 2009a; 50:224–234. [PubMed: 18775866]

Yang H, et al. 3-D histomorphometry of the normal and early glaucomatous monkey optic nerve head: lamina cribrosa and peripapillary scleral position and thickness. Invest Ophthalmol Vis Sci. 2007b; 48:4597–4607. [PubMed: 17898283]

Yang H, et al. Deformation of the normal monkey optic nerve head connective tissue after acute IOP elevation within 3-D histomorphometric reconstructions. Invest Ophthalmol Vis Sci. 2009b; 50:5785–5799. [PubMed: 19628739]

Yang H, et al. Deformation of the early glaucomatous monkey optic nerve head connective tissue after acute IOP elevation in 3-D histomorphometric reconstructions. Invest Ophthalmol Vis Sci. 2011a; 52:345–363. [PubMed: 20702834]

Yang H, et al. Posterior (outward) migration of the lamina cribrosa and early cupping in monkey experimental glaucoma. Invest Ophthalmol Vis Sci. 2011b; 52:7109–7121. [PubMed: 21715355]

Yiu G, et al. Characterization of the choroid-scleral junction and suprachoroidal layer in healthy individuals on enhanced-depth imaging optical coherence tomography. JAMA Ophthalmol. 2014; 132:174–181. [PubMed: 24336985]

Zhang X, et al. Dual-band spectral-domain optical coherence tomography for in vivo imaging the spectral contrasts of the retinal nerve fiber layer. Opt Express. 2011; 19:19653–19659. [PubMed: 21996906]

Zhi Z, et al. Volumetric and quantitative imaging of retinal blood flow in rats with optical microangiography. Biomed Opt Express. 2011; 2:579–591. [PubMed: 21412463]

Zhi Z, et al. Impact of intraocular pressure on changes of blood flow in the retina, choroid, and optic nerve head in rats investigated by optical microangiography. Biomed Opt Express. 2012; 3:2220–2233. [PubMed: 23024915]

Zotter S, et al. Visualization of microvasculature by dual-beam phase-resolved Doppler optical coherence tomography. Opt Express. 2011; 19:1217–1227. [PubMed: 21263663]

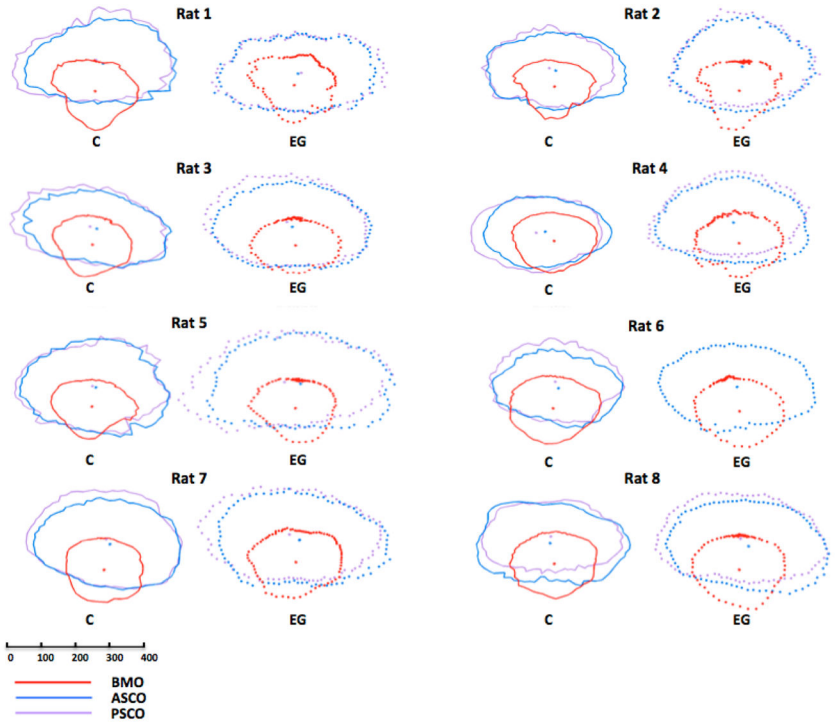

Figure 1. Within and between-eye comparisons of BMO (red), ASCO (blue) and PSCO (purple) for the Control (solid lines) and EG (dotted lines) eye of each animal

Delineated points for each structure along with their centroid are shown in right eye orientation projected onto the BMO reference plane (x axis horizontal and y axis vertical) for comparison purposes. The BMO centroid for each eye has been used to horizontally align the data for the two eyes of each animal. Note that the ASCO and PSCO centroids tend to be vertically separated and further away from the BMO centroid in the EG eyes with the greatest damage (Rats 4, 5, 7 and 8). These data suggest that apart from the EG eye expansion of these individual openings (demonstrated most clearly in Supplemental Figures 8, 9 and 10), glaucomatous alteration of the rat neurovascular scleral canal includes a vertical shift of the PSCO relative to the ASCO and BMO which becomes more pronounced as ON damage progresses. The scale is in micrometers. PSCO data is not available for the EG eye of Rat 6. Animal specific EG vs Control Eye overlays for each individual parameter can be seen in Supplemental Figures 8–10.

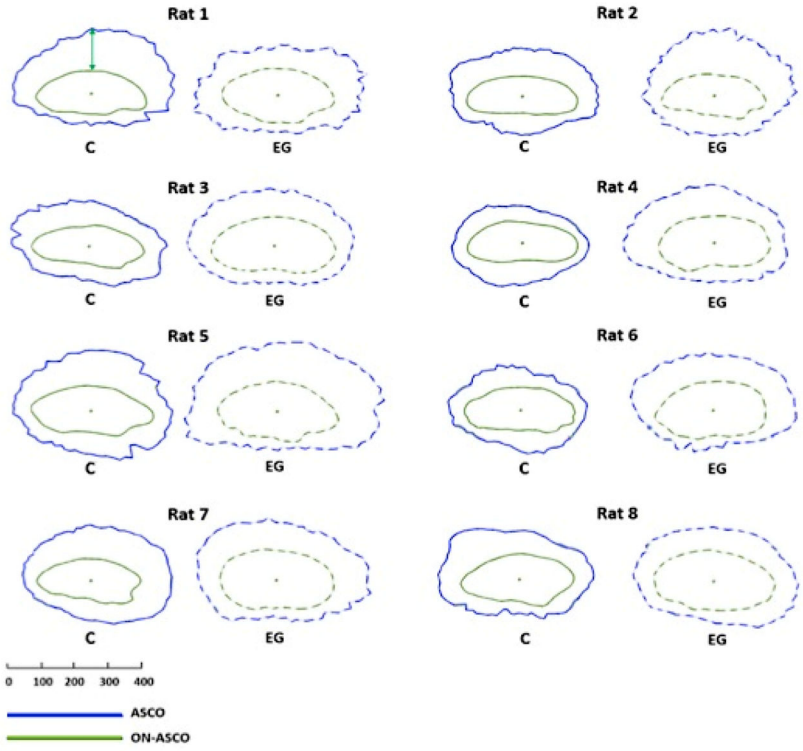

Figure 2. Animal-specific, EG (dotted line) versus Control Eye (solid line) comparisons of Anterior Scleral Canal Opening (ASCO - blue) and Optic Nerve – ASCO (ON-ASCO - green) and the ASCO-to- Optic Nerve ASCO Gap Distance (ASCO-ON-ASCO) (green arrow upper left)

ASCO fitted spline and ON-ASCO fitted spline were projected onto the ASCO reference plane for comparison purposes. The ON-ASCO centroid for each eye has been used to horizontally align the data from each eye. The green arrow (Control eye of Rat 1, upper left) schematically depicts the *ASCO-ON-ASCO Gap Distance* measurement (here showing 1 of a total of 80 radial measurements – see methods). Animal- specific EG vs Control eye overlays of ASCO and ON-ASCO data can be seen in Supplemental Figures 9 and 11, respectively. Global EG eye increases in *ASCO radius* were present within Animals 2–8. Global EG eye increases in *ON-ASCO radius* were present within Animals 1 and 3–8. Global EG eye *ASCO-ON-ASCO Distance* was significantly increased within Animals 2, 4, 5, 6 and 7. The scale is in micrometers. See Supplemental Figure 11 for a similar plot of PSCO and ON-PSCO data.

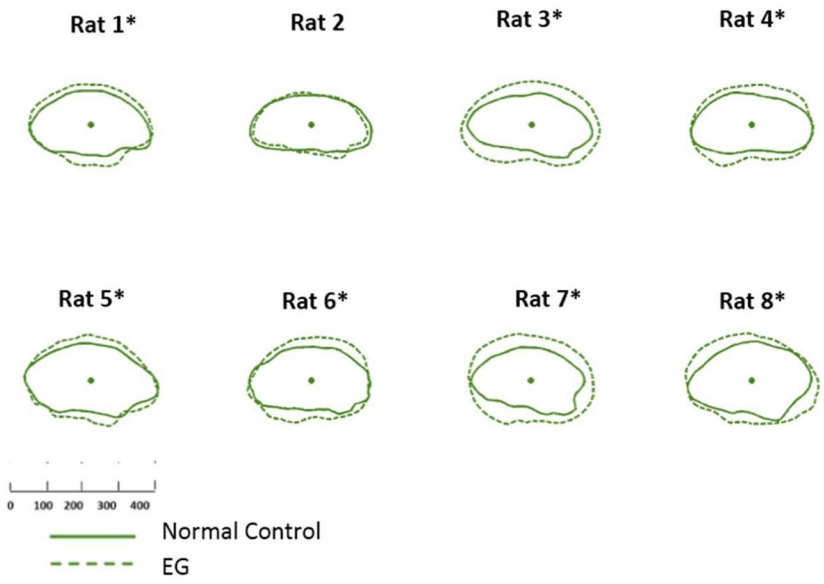

Figure 3. EG (dotted line) versus Control (solid line) eye *Optic Nerve within the Anterior Scleral Canal Opening* (*ON-ASCO)* comparison for each study animal

ON-ASCO data points for the Control and EG eye of each rat are schematically overlaid using the ON-ASCO centroid of each eye. All data are in right eye orientation. The scale is in micrometers. **(*)** denotes animals in which Global EG versus Control Eye *ON-ASCO radius* differences achieved significance (Supplemental Table 2).

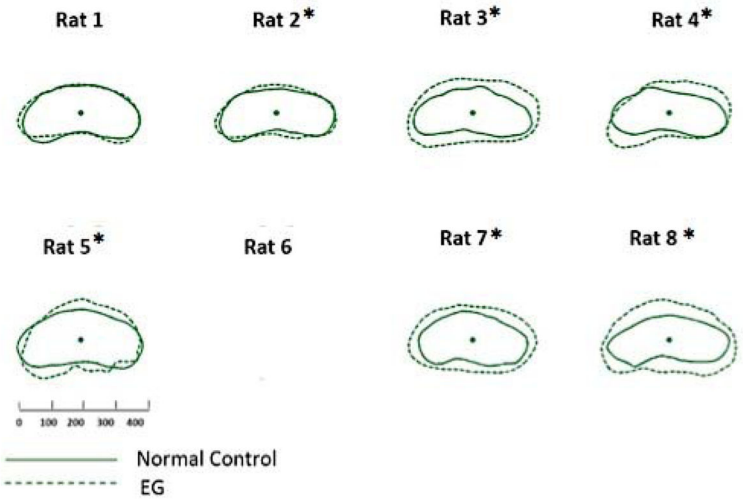

Figure 4. EG (dotted line) versus Control (solid line) eye *Optic Nerve within the Posterior Scleral Canal Opening* (*ON-PSCO)* comparison for each study animal

ON-PSCO data points for the Control and EG eye of each rat are schematically overlaid using the ON-PSCO centroid of each eye. All data are in right eye orientation. The scale is in micrometers. **(*)** denotes animals in which Global EG versus Control Eye *ON-PSCO radius* differences achieved significance (Supplemental Table 2). ON-PSCO data for EG eye of Rat 6 were not available.

Figure 5. Correlation between EG Eye *ON-PSCO Area* Expansion and EG eye *Optic Nerve Damage Grade* (Table 1)

EG vs Control eye *ON-PSCO Area* expansion was significantly correlated to EG eye *Optic Nerve Damage Grade* (R= 0.768, P=0.042). [1]Optic nerve qualitative damage grading adapted from (Morrison et al., 1997).

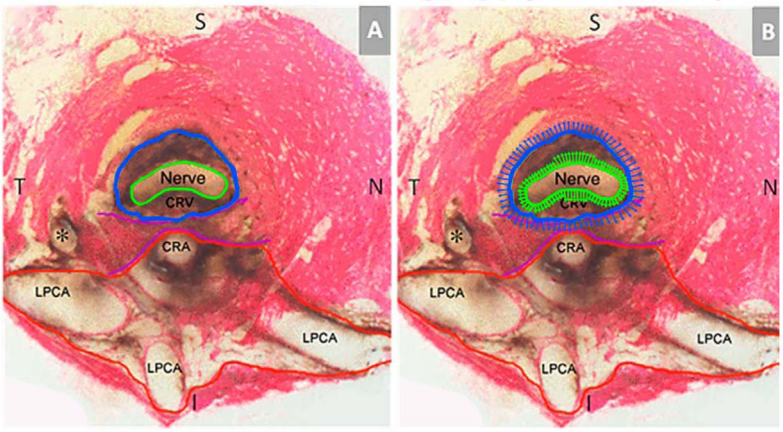

Figure 6. Principal Scleral Openings in the Normal Control Rat Eye (A) and a Schematic Overlay of Optic Nerve and Surrounding Neurovascular Scleral Canal Expansion in Early Experimental Glaucoma (EG) (B)

(A) Unlike the primate, there are two principal openings within the sclera of the rat ONH: 1) the superior neurovascular canal (outlined in blue) which contains the optic nerve (green) and the central retinal vein **(CRV)** which both pass within a vascular plexus (brown pigment) that is continuous with the choroid (not shown); and 2) the more inferior arterial opening (outlined in red), which is irregular and contains the central retinal artery (CRA) and the densely packed choroidal branches of the Long Posterior Ciliary Arteries (LPCAs). The two canals are separated by the scleral sling (purple). For a more extensive description of this anatomy see Supplemental Figures 1 and 2. **(B)** Rat optic nerve expansion (green arrows) occurs early in the rat ONH response to chronic experimental IOP elevation and is accompanied by expansion of the surrounding neurovascular scleral canal (blue arrows) that is both more frequent and of greater magnitude within the superior and inferior quadrants. Each arrow represents the magnitude of quadrant change magnified 3 times. S-superior, I – Inferior, N – Nasal, T – Temporal. (*) Identifies a branch of a LPCA.

Table 1

Abbreviations, Terms and Definitions

Abbreviation/Term	Meaning/Definition
Animal-specific results	Animal-specific EG vs Control eye Difference
ANOVA	Analysis of Variance
ASCO	Anterior Scleral Canal Opening
ASCO-ON-ASCO	Gap distance measured radially between the ASCO and the ON-ASCO
BMO	Bruch's Membrane Opening
CI	Confidence Interval
CRA	Central Retinal Artery
CRV	Central Retinal Vein
Eye-specific results	Parameters related to an individual eye
Global Results	Non-regionalized ONH or scleral data
GLS	Generalized Least Squares
H/V	Horizontal/Vertical Ratio
I	Inferior
ICC	Intraclass Correlation Coefficient
IOP	Intraocular Pressure
LPCA	Long Posterior Ciliary Artery
N	Nasal
NA	Not Available or Not Applicable
OA	Ophthalmic Artery
OD	Right Eye
OS	Left Eye
ON-ASCO	Optic Nerve area at the level of ASCO
ON-PSCO	Optic Nerve area at the level of PSCO
ONH	Optic Nerve Head
Overall results	Data from all rats considered together
PSCO	Posterior Scleral Canal Opening
PSCO-ON-PSCO	Gap distance measured radially between the PSCO and the ON-ASCO
S	Superior
SD	Standard Deviation
SPCA	Short Posterior Ciliary Artery
T	Temporal

Table 2

Animal and Eye Data.

Rat Number	ID	Age at sacrifice *(months)*	Eye	Status	Mean IOP *(mmHg)*	Mean IOP difference *(mmHg)*	EG Eye Peak IOP *(mmHg)*	Optic Nerve Damage Grade	Number of Serial Section Images
1	MR8	9.5	OD	C	28.5	5		1	400
			OS	EG	33.5		42.3	1.22	383
2	MR10	9.5	OD	EG	29.2	0.4	45	1.6	465
			OS	C	28.8			1	313
3	MR1	9.5	OD	EG	33.3	5	39.1	2	696
			OS	C	28.3			1	398
4	MR9	9.5	OD	EG	35	6.6	45.8	2.36	430
			OS	C	28.4			1	307
5	MR12	10.5	OD	EG	29.6	1.1	36	2.47	500
			OS	C	28.5			1	275
6	MR11	10.5	OD	EG	32.1	3.8	41	2.9	230
			OS	C	28.3			1	375
7	MR5	9.5	OD	C	28.8	3.7		1	484
			OS	EG	32.5		40.9	3	480
8	MR4	9.5	OD	C	28.4	6.2		1	501
			OS	EG	34.6		42.3	3.28	455

ID – Laboratory Rat Identification Number; **Age**- in months; **Eye** - OD-Right eye, OS-left eye**; Status**- C- Control, EG-Experimental Glaucoma; **Mean IOP** (mmHg)- Mean IOP of all IOP measurements taken AM and PM for each eye**; Mean IOP difference**- Mean IOP of the EG eye minus Mean IOP of the Contol eye (mmHg). **EG Eye Peak IOP** - Maximum IOP in mmHg obtained in the EG eye; **Optic Nerve Damage Grade:** average score of orbital optic nerve cross section grading performed by 5 masked observers using a previously published scale (Morrison *Exp. Eye Res.* 1997). **Number of Digital Serial Section Images**- number of serial digital section images required to reconstruct each optic nerve head.

Table 3

Overall Global Values for each Parameter by Treatment Group

Parameters	Control Eyes (Mean±SD)	EG Eyes (Mean±SD)	P-Value
Neurovascular Canal			
BMO Area (μm²)	5.65±0.66×10⁴	6.13±0.51×10⁴	0.0375
BMO Radius (μm)	133±8	139±6	0.0358
BMO Depth (μm)	29±15	35±12	0.3448
ASCO Area (μm²)	1.29×10⁵±0.19 ×10⁵	1.60×10⁵±0.21 ×10⁵	**0.0016***
ASCO Radius (μm)	201±15	224±14	**0.0016***
ASCO H/V Diameter Ratio	1.26±0.10	1.24±0.11	0.6974
ASCO Depth (μm)	95±14	92±16	0.5450
PSCO Area (μm²)[1]	1.35×10⁵±0.23 ×10⁵	1.67×10⁵±0.27 ×10⁵	0.0118
PSCO radius (μm)[1]	206±17	229±17	0.0104
PSCO H/V Diameter Ratio[1]	1.28±0.14	1.22±0.12	0.4276
PSCO Depth (μm)[1]	165±13	162±15	0.6787
Optic Nerve			
ON-ASCO Area (μm²)	4.63×10⁴±0.44×10⁴	6.13×10⁴±0.94×10⁴	**0.0021***
ON-ASCO Radius (μm)	118±6	137±12	**0.0012***
ON-ASCO H/V Diameter Ratio	1.96±0.19	1.60±0.16	**<0.001***
ON-PSCO Area (μm²)[1]	4.42×10⁴±0.48×10⁴	6.07×10⁴±0.98×10⁴	0.0089
ON-PSCO Radius (μm)[1]	111±7	134±12	0.0066
ON-PSCO H/V Diameter Ratio[1]	2.38±0.43	2.21±0.35	0.4971
ON Volume (μm³)[1]	3.29×10⁶±0.64×10⁶	4.59×10⁶±0.90×10⁶	0.0175
Optic Nerve/Scleral Canal Gap Distance			
ASCO-ON-ASCO Distance (μm)	81±13	85±13	0.4080
PSCO-ON-PSCO Distance (μm) [1]	93±13	94±15	0.8342
Sclera/Choroid			
Scleral Thickness (μm)[1]	104±4	104±4	0.8265
Scleral Depth (μm)	33±7	35±7	0.5296
Choroidal Thickness (μm)	57±7	52±11	0.3142

Statistical significance was defined to occur at the *p<0.0022 (Paired T-Test) due to multiple comparisons;

[1]These parameters calculations were obtained without rat 6 data

EG- Experimental Glaucoma

Table 4

Frequency of Animal-Specific EG Eye Global Change for each Parameter

Parameter[1]	Number of Rats Demonstrating EG Eye Change[2]		Range of significant EG Eye Change (%)[3]	
	+	-	+	-
Neurovascular Canal				
BMO Radius (μm)	5	0	5 ~ 13 *(3 ~ 10)*	0 *(0)*
BMO Depth (μm)[4]	5	2	2 ~ 28	−21 ~ −12
ASCO Radius (μm)	7	0	16~ 38 *(8 ~ 21)*	0 *(0)*
ASCO Depth (μm)	1	2	16	−30 ~ −18
PSCO Radius (μm)[4]	6	0	10 ~ 43 *(5 ~ 21)*	0 *(0)*
PSCO Depth (μm)[5]	3	4	11 ~ 18	−28 ~ −7
Optic Nerve				
ON-ASCO Radius (μm)	7	0	14 ~ 34 *(11 ~ 30)*	0 *(0)*
ON-PSCO Radius (μm)	6	0	9 ~ 43 *(8 ~ 41)*	0 *(0)*
Optic Nerve to Scleral Canal Gap Distance				
ASCO-ON-ASCO Distance (μm)	4	1	14 ~ 17 *(18 ~ 26)*	−12 *(−13)*
PSCO-ON-PSCO Distance (μm)[4]	2	2	14 ~ 28 *(18 ~ 29)*	−17~ −10 *(−16 ~ −10)*
Sclera/Choroid				
Scleral Thickness (μm)[4]	3	2	4 ~ 6 *(4 ~ 5)*	−9 ~ −7 *(−8 ~ −7)*
Scleral Depth (μm)	4	1	6 ~ 10	−10
Choroidal Thickness (μm)	2	6	4 ~ 19 *(8 ~ 32)*	−20 ~ −5 *(−29 ~ −7)*

[1] Only parameters in which multiple measurements per eye were possible were included in this analysis

[2] Between eye comparison (EG versus control) was carried out for each parameter for each animal using generalized least squares model (GLS). Statistically significant between-eye differences were established at $p<0.005$ due to multiple comparisons. Positive sign (+) means increased, negative sign (−) means reduction.

[3] The range of statistically significant EG eye change in micrometers. Percentage is in parentheses *(expressed as the percent of the contralateral control Eye).* Positive sign (+) means increased, negative sign (−) means reduction.

[4] This parameter could only be measured in 7 of the 8 animals

Table 5

Overall Regional Values for each Parameter by Treatment Group

Parameters	Superior		Inferior		Nasal		Temporal	
	C (Mean±SD)	EG (Mean±SD)	C (Mean±SD)	EG (Mean±SD)	C (Mean±SD)	EG (Mean±SD)	C (Mean±SD)	EG (Mean±SD)
Neurovascular Canal								
BMO Radius	135±10	141±10	138±15	143±18	132±11	137±11	128±16	136±17
BMO Depth	27±13	31±14	32±17	39±13	32±16	39±14	26±18	32±14
ASCO Radius	187±22	**208±18** *	186±21	205±19	217±22	244±24	214±19	**240±22** *
ASCO Depth	83±15	78±15	113±20	111±18	101±17	93±20	84±22	85±22
PSCO Radius	196±25	214±21	188±22	203±20	213±22	246±29	222±23	252±32
PSCO Depth	145±16	135±14	189±19	191±20	177±24	171±28	152±20	151±22
Optic Nerve								
ON-ASCO Radius	98±9	**121±13** *	90±14	116±17	141±20	156±18	142±22	156±19
N-PSCO Radius	86±10	**111±15** *	68±12	94±20	145±31	165±26	146±29	164±29
Optic Nerve to Scleral Canal Gap Distance								
ASCO-ON-ASCO Distance (μm)	107±32	117±27	75±21	57±18	72±28	86±30	72±26	82±26
PSCO-ON-PSCO Distance (μm)	115±32	113±27	112±22	97±15	60±35	73±30	82±31	95±35
Sclera/choroid								
Scleral Thickness	99±14	98±15	91±20	91±19	113±19	113±16	116±23	112±21
Scleral Depth	30±25	29±22	41±31	46±32	37±27	37±30	22±26	28±28
Choroidal Thickness	57±11	49±16	56±14	51±18	59±22	51±15	55±15	58±25

* Statistically significant EG versus Control Eye difference established at $p<0.0125$ due to multiple comparisons (linear mixed effects model)

All values are in micrometers.

Table 6

Frequency of Animal-Specific EG Eye Regional Change for each Parameter.

Parameters	Superior				Inferior				Nasal				Temporal			
	# of Animals[1]		Range of EG Eye Change (%)[2]		# of Animals[1]		Range of EG Eye Change (%)[2]		# of Animals[1]		Range of EG Eye Change (%)[2]		# of Animals[1]		Range of EG Eye Change (%)[2]	
	+	−	+	−	+	−	+	−	+	−	+	−	+	−	+	−
Neurovascular Canal																
BMO Radius	3	0	13 ~ 18 *(9 ~15)*	0*(0)*	2	0	15 ~ 19 *(11~ 15)*	0 *(0)*	2	0	11 ~19 *(9 ~15)*	0 *(0)*	2	0	10 ~ 17 *(7 ~ 14)*	0 *(0)*
BMO Depth	3	2	18 ~ 20	−16 ~ −13	4	2	6 ~ 36	−22 ~−16	4	3	14 ~37	−18 ~−8	4	2	4 ~ 30	−26 ~−10
ASCO Radius	7	1	14 ~44 *(7 ~ 26)*	−21 *(−10)*	5	0	22 ~36 *(13 ~ 20)*	0 *(0)*	5	0	23~63 *(11 ~28)*	0 *(0)*	5	0	15 ~48 *(7 ~ 23)*	0 *(0)*
ASCO Depth	2	2	11 ~14	−36 ~−22	1	2	28	−31 ~−15	1	4	31	−30 ~ −14	2	2	15 ~ 25	−25 ~−21
PSCO Radius	5	0	25 ~ 37 *(12 ~22)*	0 *(0)*	3	0	26 ~42 *(15 ~ 27)*	0 *(0)*	5	0	18 ~71 *(8~ 32)*	0 *(0)*	5	0	15 ~ 57 *(6 ~24)*	0 *(0)*
PSCO Depth	0	3	0 *(0)*	−25 ~−15	2	1	17 ~ 33	−26	1	3	33	−36 ~−23	2	2	21 ~ 37	−28 ~−24
Optic Nerve																
ON-ASCO Radius	8	0	5~ 35 *(5 ~ 37)*	0 *(0)*	8	0	9 ~ 39 *(11 – 44)*	0 *(0)*	4	0	14 ~32 *(10 ~ 24)*	0 *(0)*	4	0	13 ~ 30 *(9 ~23)*	0 *(0)*
ON-PSCO Radius	6	0	13~46 *(16 ~ 57)*	0 *(0)*	5	0	25 ~ 48 *(36–79)*	0 *(0)*	3	0	31~ 40 *(23 ~ 28)*	0 *(0)*	3	0	29 ~ 39 *(21~ 27)*	0 *(0)*
Optic Nerve to Scleral Canal Gap Distance																
ASCO-ON- ASCO Distance	5	1	18~49 *(16~78)*	−66*(−43)*	0	5	0 *(0)*	−41~ −19 *(−47~ −24)*	4	0	17~52 *(26 ~ 77)*	0 *(0)*	3	1	13 ~34 *(20 ~ 54)*	−30 *(−32)*
PSCO-ON- PSCO Distance	3	3	19~47*(20~55)*	−61~−13*(−39~−14)*	1	2	25 *(28)*	−52 ~−23 *(−37 ~−18)*	2	1	26~68 *(64~140)*	−58 *(−50)*	2	1	52~ 56 *(60 ~ 83)*	−27 *(−24)*
Sclera/choroid																
Scleral Thickness	2	2	9 ~ 10 *(11 ~ 12)*	−22 ~−6 *(−20 ~−6)*	2	1	9 ~ 15 *(10 ~ 18)*	−10 *(−11)*	1	0	7 *(7)*	0 *(0)*	0	2	0	−20 ~−18 *(−15)*
Scleral depth	1	2	14	−21 ~−9	1	0	23	0	0	0	0	0	3	1	14 ~23	−13
Choroidal Thickness	1	6	19 *(31)*	−21~−4 *(−35 ~−7)*	1	5	19 *(33)*	−21~−7 *(−36 ~−12)*	2	4	8 ~ 10 *(16 ~25)*	−44~−10*(−47~−19)*	3	4	5 ~ 21 *(11 ~36)*	−22 ~−7 *(−37 ~−11)*

Statistical significance for regional parameter change within each animal was required to achieve $p<0.0001$ due to multiple comparisons (linear model using generalized least squares) Values are in microns or *(percent in parentheses)*

[1] number of animals achieving statistically significant change in this parameter within this region. Positive sign (+): increase. Negative sign (−): reduction.

[2] range of the statistically significant EG eye change in micrometers and percentage % *(reported as the percent of the contralateral normal eye)* Positive sign (+): increase. Negative sign (−): reduction.